

EPTT-2020-0067

**EXPERIMENTAL INVESTIGATION OF INITIAL DISTURBANCES
FORMATION, INSTABILITIES GROWTH, MULTIPHASE TURBULENCE
AND BREAKUP MECHANISM INSIDE A MIXING CHAMBER OF AN AIR-
ASSIST ATOMIZER**

Vinícius Basso de Godoy*

viniciusbassodegodoy@gmail.com

Diogo Alexandre Santos*

diogoalexsantos@hotmail.com

Bárbara Braatz Vetter*

barbarabraatz.vetter@gmail.com

Lilian Rodrigues Canabarro

Petróleo Brasileiro S.A. – Research and Development Center (CENPES) – Rio de Janeiro – RJ

lilian.canabarro@petrobras.com.br

Leonardo Machado da Rosa*

leorosa@gmail.com

Marcela Kotsuka da Silva*

marcelakotsuka@furb.br

Jonathan Utzig*

jutzig@furb.br

Henry França Meier*

meier@furb.br

*Chemical Engineering Department – University of Blumenau (FURB) – Blumenau – SC

Abstract. *The purpose of this paper is to perform a preliminary study in the formation of initial disturbances, the growth of instabilities, multiphase turbulence and the primary breakup mechanism that arises inside an air-assist atomizer. To achieve such goal, a mixing chamber device was used on the experiments. This device is composed in such a way that allows for visual techniques to be employed. The experiments were performed using water at 365 kg/h and air as atomizing fluid at 40 kg/h. These operational conditions resulted in a Reynolds number of 10398, a Weber number of 308, an Ohnesorge number of 0.0017, an aerodynamic Weber number of 17697, and a Mach number approximately equal to 2.7, indicating that the air flow is supersonic. Flow visualization was executed with a high-speed camera at resolutions between 96x64 and 640x1024 pixels, image acquisition rate between 5000 and 58099 frames per second, and exposure time of 8 μ s. The pseudo-two-dimensional device allowed for the flow visualization and proved to be effective. With this study, it was possible to observe the initial instabilities and turbulences inside the mixing chamber. The images outside the chamber provided an estimation of spray angle, droplet diameters and ligaments lengths.*

Keywords: *atomization, primary breakup, visual techniques, air-assist atomizer, multiphase turbulence*

1. INTRODUCTION

Atomization, which consists on the transformation of bulk liquids into different droplet sizes, is widely used in many applications. According to Lefebvre and McDonell (2017), the major reason for this statement is mainly due to an increment on superficial area of the liquid that is being fragmented. For instance, an important process deriving from the oil refining industry, known as Fluid Catalytic Cracking or FCC, utilizes this increase in area to enhance the mechanisms of heat and mass transport between vapor, gasoil and catalyst contained in the reactor. This promotes a more

efficient process, since more gasoil is converted to high added-value products such as high-octane gasoline, jet fuel and diesel (Sadeghbeigi, 2012).

Additionally, the atomization phenomenon can be divided into two different stages of breakup, the primary and secondary breakup. The former is a product of the competition between the stabilizer influences of tension force and viscosity and disruptive influences of fluid dynamic instabilities, large drag forces and multiphase turbulence (Lefebvre and McDonell, 2017). When disruptive overcome stabilizer influences, initial disturbances are promoted on the gas-liquid interface, followed by growth in liquid body oscillations and subsequently liquid disintegration into ligaments and drops, as investigated by Saha et al. (2012), Davanlou et al. (2015) and Ghasemi et al. (2020). The breakup stage known as secondary breakup consists of the deformation and disintegration of larger droplets formed on primary breakup into smaller droplets due to aerodynamics instabilities generated mainly by random fluctuations of velocity components, air drag and relative velocity between droplets and the environment (Saha et al., 2012).

These stages are accomplished by devices recognized as atomizers. A class widely applied in FCC process is the air-assist atomizer because of its efficiency on breaking up liquids with high viscosity (Lefebvre and McDonell, 2017). The above-mentioned atomizers consist of exposing a liquid to a high-velocity air or vapor stream with the mixing of both phases occurring inside the device. It is also known that the gaseous phase can reach supersonic velocities. Among other factors, when strong velocity gradient occurs, turbulent shear layers are generated on the liquid interface. Consequently, by the unstable nature of the flow, turbulent flow structures such as Kelvin-Helmholtz (K-H) instabilities also rises on the interface (Ghasemi et al., 2020). The K-H mechanism can be considered one of the many causes of ligament and droplet formation on these atomizers, essentially giving birth to the primary breakup mentioned above.

However, as many atomizers are manufactured with pressure-resistant materials, usually metals, the observation of initial discrete portions of fluid being detached from liquid bulk that occurs inside the atomizer body becomes unfeasible. Thus, the objective of this paper is to perform a preliminary study not only on the formation of initial disturbances, but also on the growth of instabilities, multiphase turbulence and primary breakup mechanism that arises inside the atomizer. To achieve such goal, a pseudo-two-dimensional device, which represents the mixing chamber, was used on the experiments. This device is composed in such a way that allows high-speed camera imaging technique to be employed of both mixing chamber and downstream region of the nozzle. Similar transparent devices were implemented by Cui et al. (2017) and Murugan et al. (2020), where the internal flow patterns were successfully defined. In the present study, the experiments were performed using water as the liquid to be atomized and air as the atomizing gas. Qualitative results such as regions with K-H instabilities, shear layer and discrete liquid structure formation are presented and discussed. Moreover, estimations on droplet size, ligament length and spray angle were measured in order to characterize the phenomenon.

2. METHODOLOGY

Experiments were conducted at Verification and Validation Laboratory of the University of Blumenau (FURB) in an experimental facility designed for spray studies. Figure 1 depicts a schematic of the atomization test facility, which is composed of water and compressed air loops, pseudo-two-dimensional atomizer, measurement and data acquisition systems, water collector, water reservoir, and an atomizing chamber.

The water loop consists of a Schneider BC-92T 1A 1.5 HP centrifugal pump controlled by a Schneider Electric ATV310HU75N4E variable frequency inverter, a Venturi flowmeter that is formed by a Venturi tube and a differential pressure transducer (Rücken RTBP-420-DIF), a Danfoss MBS 1700 gauge pressure transducer, and a PT-100 KSE STS-A11 temperature sensor attached to a 4 to 20 mA transmitter. The last two sensors are installed next to the atomizing device. The temperature and differential pressure data from the water loop were used to calculate the water mass flow rate.

Ambient air is supplied by a Motomil MAV 30/250 7.5 HP piston compressor, with a maximum gauge pressure of 12 bar and a maximum theoretical flow rate of 885 L/min at an air density of 1.13 kg/m³. Initially, the compressed air passes through two sets of filter regulators that regulate the air pressure and remove both dust particles and humidity. Subsequently, the air pressure is regulated again by an AIRTAC IR2020-02 precision air pressure regulator with an operating pressure of 1 to 9 bar. The air flow rate, in which is measured by a Techmeter TCM-7.000 variable area flowmeter, is controlled by a ball valve installed downstream of the meter. In order to assure proper calculation of mass flow rate from the air loop, a prior calibration was conducted in the system that correlates pressure, temperature and observed volumetric flow rate. For this reason, were also installed a Danfoss MBS 1700 gauge pressure transducer and a PT-100 KSE STS-A11 temperature sensor downstream and upstream of the flowmeter, respectively.

The sensor electronic measurements were obtained by a data acquisition system, in which consists of a National Instruments (NI) USB-6001 acquisition card installed in a laptop and a developed LabVIEW 15.0 acquisition program. For this study, the water and air mass flow rates were defined as 365 kg/h at 123.0 kPa and 40 kg/h at 403.0 kPa, respectively, both at room temperature.

The atomization phenomenon is typically analyzed through dimensionless numbers, such as Reynolds number ($Re = \rho_w u_w L / \mu$), Weber number ($We = \rho_w u_w^2 L / \sigma$), Ohnesorge number ($Oh = (We)^{1/2} / Re$), and aerodynamic Weber

number ($We_a = \rho_g (u_g - u_w)^2 L / \sigma$). In this study, ρ_w is the water density, u_w is the water velocity at the inlet, ρ_g is the air density, u_g is the air velocity at the inlet, L is the side of the water inlet, μ is the water viscosity, and σ is the water surface tension. The Reynolds number represents the ratio between inertial and viscous forces and it indicates the occurrence of turbulence on a flow. The Ohnesorge number relates viscous forces with combined forces of inertia and surface tension and it is directly proportional to liquid jet instability. Additionally, the Weber numbers represent the ratio between inertial and surface tension forces, being described as a measure of the relative importance of inertia over surface tension (Sens et al., 2012). When air flow reaches sonic or supersonic speed, the Mach number ($M = u_g/c$) is used as a measure of the flow compressibility (Kundu et al., 2012). Here, c is defined as the speed of the sound in the medium.

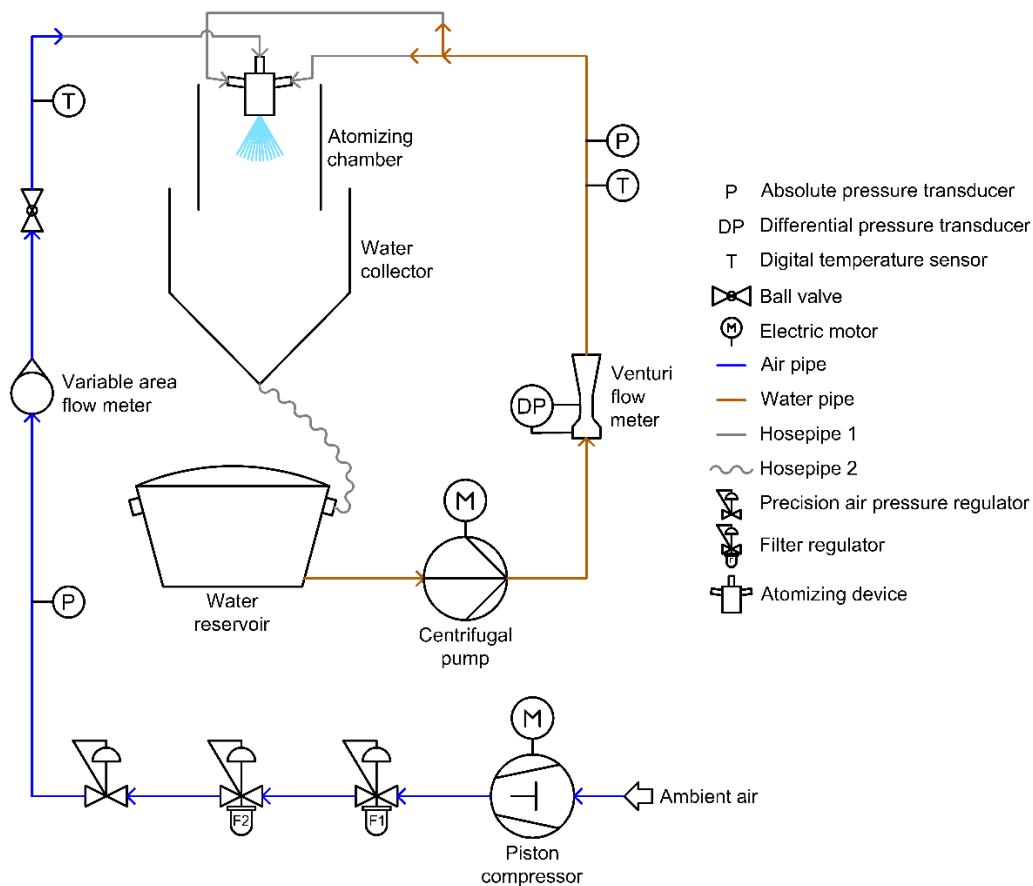


Figure 1. Atomization test facility scheme.

The atomizer represents the mixing chamber of industrial air-assisted atomizers and it is constructed in a two-dimensional way to enable the observations of two-phase interface. The mixing chamber material was SAE 1020 Steel, consisting mainly of two blocks equally machined and grinded according to Fig. 2a. The purpose of the machining was not only to shape the device, but also to form the inlets through which the fluids enter the mixing chamber. Furthermore, the two blocks are joined by a grinded contact surface, where the reason for this was to guarantee the flatness and especially the sealing, forming one single solid block with the fluid inlets as shown in Fig. 2b. In addition, the blocks are attached using screws and their outer contact faces are welded.

The mixing region of the chamber is composed of a single rectangular section, where the first contact between both fluids occurs and where the primary breakup takes place. This chamber section is approximately 60 mm of height, 17 mm of width, and 8 mm of depth. The fluids inlets have a square format, in which the air inlet has an area slightly larger than 9 mm² and the water inlets have an area of approximately 21 mm².

This sort of fabrication and assembly was particularly chosen due to the square format of the inlets, making it difficult to perform a more standard fabrication using a single block with circular inlets. Moreover, pneumatic and hydraulic connectors are used to connect the 3/4" and 1" air and water hoses, respectively. Lastly, in order to seal the internal chamber sides completely, two acrylic plates were attached laterally with screws. Figure 2c shows the finished pseudo-two-dimensional atomizer.

Detailed observations of instabilities, breakups, and oscillations were accomplished by an IDT OS3-S2 digital high-speed camera with maximum resolution of 1280x1024 pixels, maximum image acquisition rate of 5000 frames per

second at the maximum resolution and a minimum exposure time of $1 \mu\text{s}$. A Veritas Constellation 120E light source, a Metabones Speed Booster XL that regulates the light penetration on the camera sensor, and a Nikon AF-S NIKKOR lens with a focal length of 35 mm and maximum opening of $f/1.8$ were also used along with the camera. All images were processed by the IDT Motion Studio software. Figure 3 shows the image acquisition system.

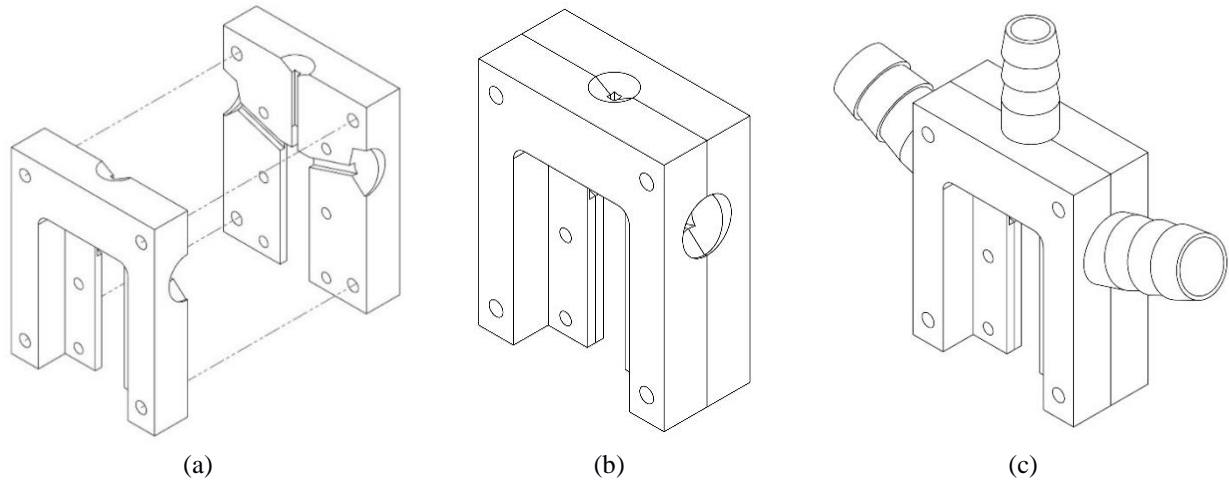


Figure 2. (a) Machined and grinded blocks, (b) attached blocks forming the mixing chamber and (c) finished pseudo-two-dimensional atomizer with connectors.

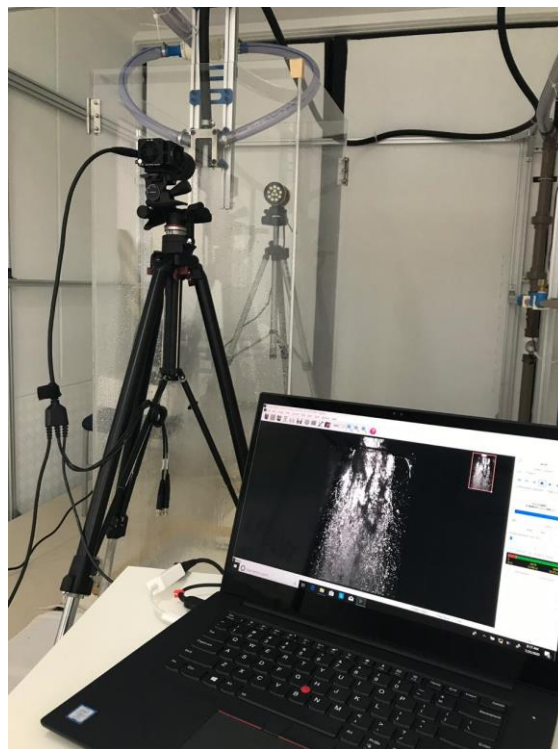


Figure 3. Image acquisition system.

In order to analyze the phenomenon completely, images of five regions were acquired as shown in Fig. 4. The different regions were selected as follows: almost the entire mixing chamber was considered Region A; the first section of the mixing chamber, exactly below the air inlet, was defined as the Region B; Region C is right below the Region B; Region D is located, in turn, right below Region C; the near-nozzle section, outside of the mixing chamber, was classified as Region E. The parameters set by the image acquisition system, such as resolution, frame rate, and image size are presented in Tab. 1. All images were acquired separately for each individual region. Additionally, the light source and the camera were arranged in a way that allowed a separation angle of 180° with each other. For this reason, gradients related to volume fraction are formed on the images, as a shadowgraphy technique: the

darker colors represent the interfaces between the fluids, while the lighter colors represent continuous phases i.e. predominantly water or air. It is worth mentioning that the areas with a solid black color refer to the atomizer's wall.

Table 1. Image acquisition parameters.

Region	Image resolution (pixels)	Frame rate (Hz)	Image size (mm x mm, approximately)
A	256 x 832	6090	20 x 60
B	96 x 64	58099	6 x 4
C	96 x 64	58099	6 x 4
D	96 x 64	58099	6 x 4
E	640 x 1024	5000	44 x 70

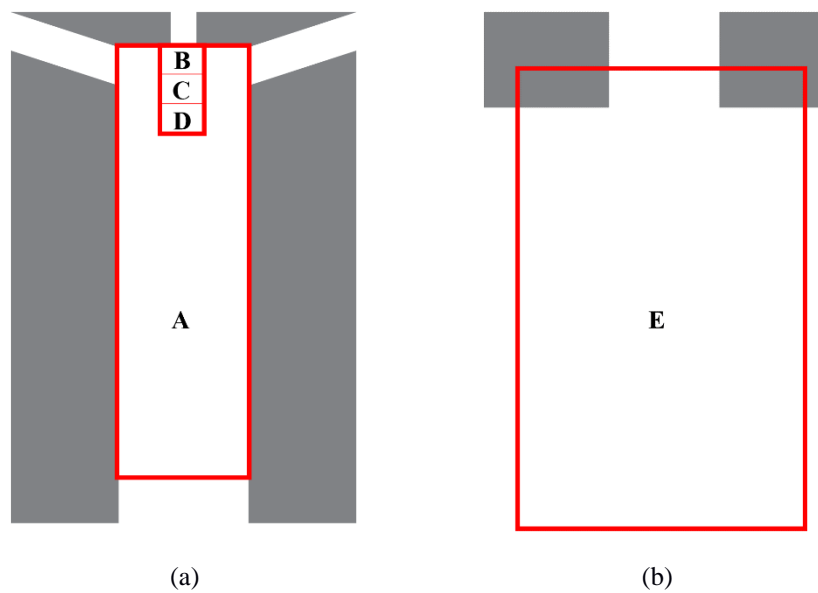


Figure 4. (a) Regions selected inside the mixing chamber and (b) region selected outside the mixing chamber.

3. RESULTS AND DISCUSSION

This section comprises two main types of results. First, the results obtained on the different regions defined previously are qualitatively analyzed, with instabilities and liquid structures identification. Then, quantitative results, such as spray angle, droplet diameters and ligament lengths are estimated, considering the region outside the mixing chamber, Region E.

Figure 5 presents the interaction between phases across almost the entire mixing chamber (Region A). It is worth noticing the presence of a cyclic flow pattern illustrated by the difference on the length of the gas core formed by air flow. When the gas core is at its maximum opening, it reaches values around 43 mm. On the other hand, when the gas core is almost entirely filled by water, its length reaches 7 mm. Thus, given the chosen experimental conditions, the phenomenon displays an unsteady behavior.

Figure 6 shows a set of instantaneous snapshots of the Region B, located right below the air inlet. As expected, the high velocity of air produces the so-called turbulent shear-layers at the interface, promoting the onset of disturbances and perturbations seen on Fig. 6a. Considering the air flow as isotropic and through converging-diverging nozzle, the M can be calculated as approximately equal to 2.7 at the mixing chamber. Comparing the fluids velocities, the air has a much greater velocity than the water (2.15 m/s), causing the formation of a velocity gradient. This strong velocity gradient formed is responsible for the K-H instabilities generated in early stages of primary breakup, as can be observed on the images shown on Fig. 6b, 6c and 6d. Although many turbulent mixing and instabilities occur in this region, only a few discrete liquid structures were formed.

As this region of analysis is short when compared to the chamber and it is right below the air inlet, the outcome of the above-mentioned instabilities should appear more frequently in the subsequent regions. This outcome can be observed on Fig. 7 and 8, in which the set of images represents instantaneous snapshots of the Region C.

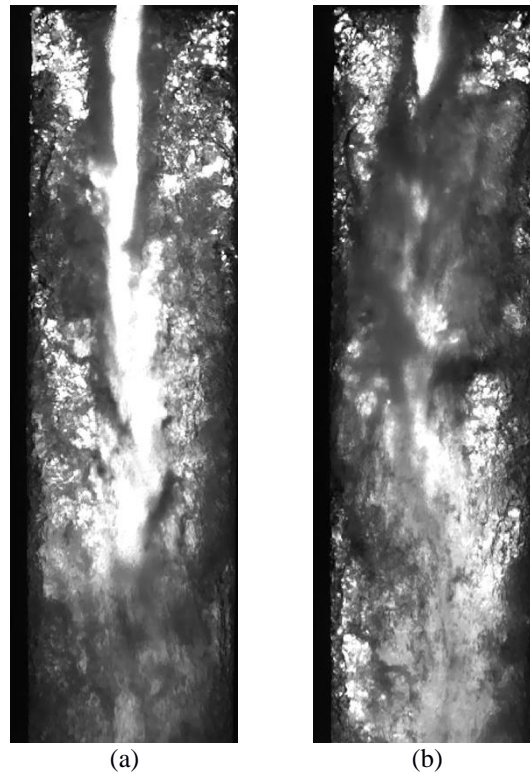


Figure 5. Unsteady flow behavior on Region A with a timestep of 9.85×10^{-4} s between snapshots.

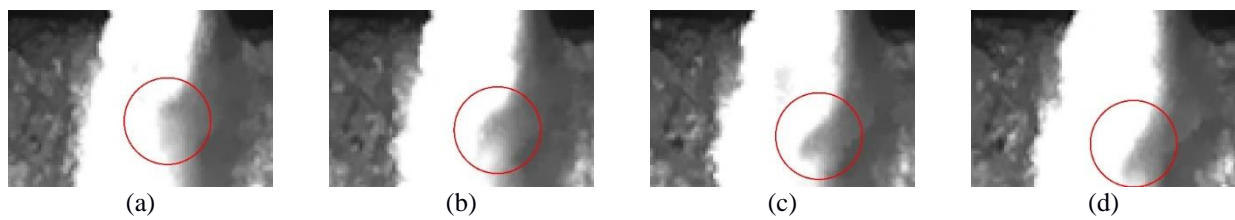


Figure 6. K-H instability formation on Region B with a timestep of 1.72×10^{-5} s between snapshots.

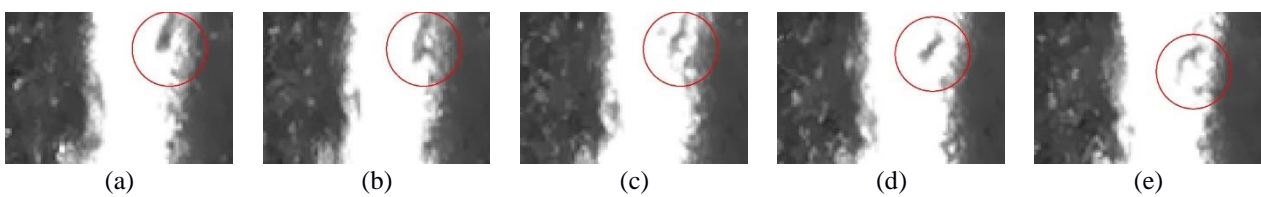


Figure 7. Ligament formation on Region C with a timestep of 1.72×10^{-5} s between snapshots.



Figure 8. Droplet formation on Region C with a timestep of 1.72×10^{-5} s between snapshots.

Figure 7 illustrates the detachment of ligaments from the liquid bulk and, although ligaments are more frequent in this region, Fig. 8 reveals that some droplets are also formed. The formation of these structures can be explained by the intensification of the K-H instabilities, turbulence and oscillations on the interface. This, in fact, characterizes the dawn of primary breakup on air-assisted atomizers, revealing the large momentum transfer between phases.

Figure 9 shows instantaneous snapshots of Region D. In this region, an even greater number of discrete liquid structures is formed, evidencing the ongoing development of the primary breakup and growth of flow turbulence.

The image analysis of these small regions (B, C and D) was indeed able to capture the dawn of primary breakup and its development.

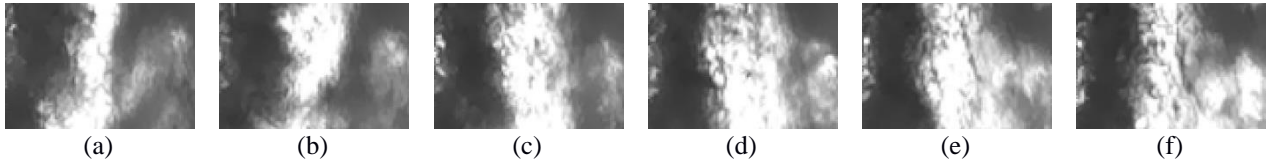


Figure 9. Liquid structures on Region D with a timestep of 3.44×10^{-5} s between snapshots.

Figure 10 shows the region right below the mixing chamber nozzle, where the flow is no longer confined. In order to characterize the atomization phenomenon of a pseudo-two-dimensional air-assisted atomizer, some preliminary estimations were made regarding important parameters defined previously.

As shown in Fig. 10a, the spray angle was calculated as 13.8° . On the other hand, the spray angle seen laterally was calculated as 10.5° , as presented by Fig. 10c. Additionally, on Fig. 10b, droplet diameters and ligament lengths ranging from roughly 200 to 680 μm and 1 to 5.8 mm were found, respectively. To ensure correct measurement of diameters, an image processing algorithm by NI Vision software was performed on four randomly selected images. Moreover, a distribution of droplet diameters from the processed images was determined and the Sauter mean diameter (D_{32}) was calculated as 352.5 μm . Figure 11 presents both the image processing algorithm and the droplet distribution curve.

It is worth mentioning that most mechanisms of breakup initiated on the mixing chamber remain present in the external region with decreased intensity due to air deceleration. On the other hand, the effect of Rayleigh-Taylor (R-T) interface instability becomes higher due to heavier fluid being pressed against a lighter stagnant gas (Sharp, 1984). This promotes further breakup of larger droplets to smaller ones. This atomization process can be also characterized by the dimensionless numbers. Considering the operational conditions applied to this study, the calculated parameters are presented on Table 2. Note that, for the calculation of aerodynamic Weber number, an approximation for the air pressure was inferred due to lack of pressure measurements near the mixing chamber inlet.

According to the breakup regime diagram proposed by Hopfinger (1998), the operating condition of this study produces a breakup in the form of fibers, named as fiber-type atomization. This regime along with high We_a may indicate that the influence of surface tension is negligible in determining the primary drop size (Lasheras and Hopfinger, 2000). As can be seen by the large Reynolds number, the strong turbulence at the inlet produces a wavy pattern on the water jet enhanced by aerodynamic effects (Hopfinger, 1998).

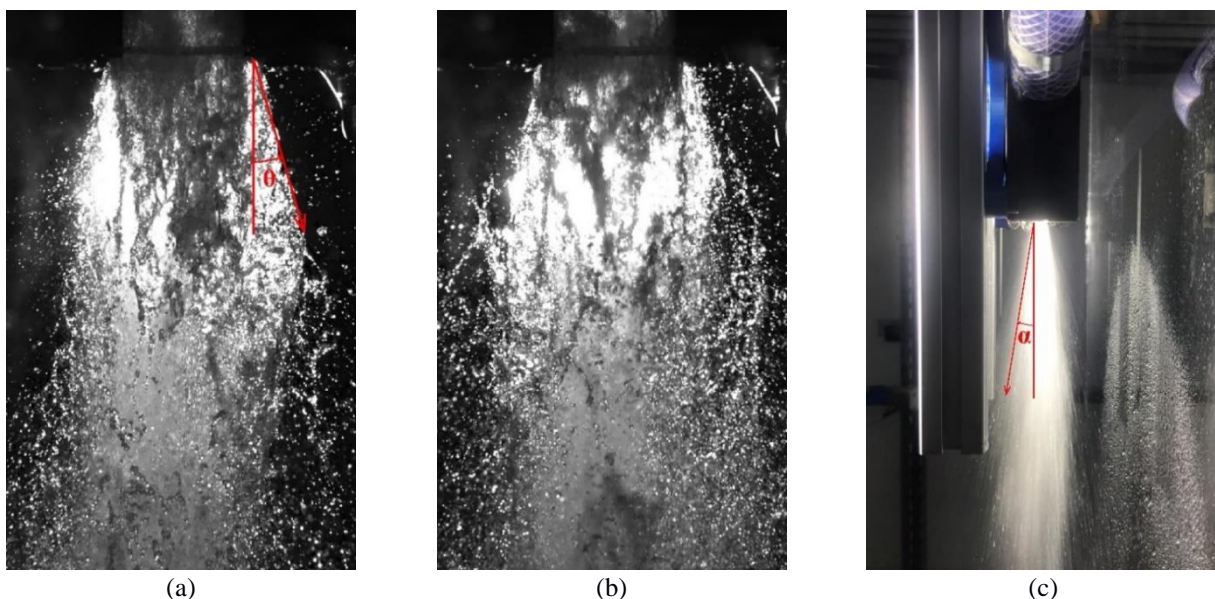


Figure 10. Spray characterization on Region E.

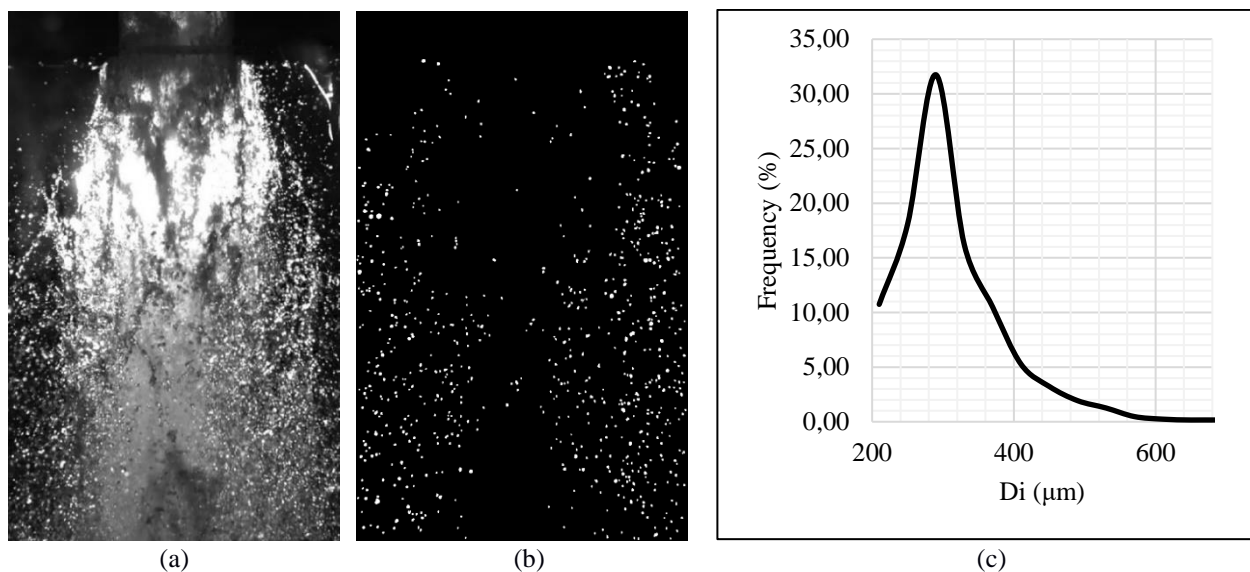


Figure 11. (a) Original image, (b) filtered image and (c) droplet distribution curve.

Table 2. Calculated dimensionless numbers.

Dimensionless number	Calculated value
Re	10398
We	308
Oh	0.0017
We_a	17697

4. CONCLUSIONS

A preliminary study was conducted in order to evaluate mechanisms of breakup inside a pseudo-two-dimensional mixing chamber on an air-assisted atomizer and its effect on spray characteristics. For this purpose, experiments were applied using air at 40 kg/h and water at 365 kg/h with Re of 10398, We of 308, Oh of 0.0017, We_a of 17697, and M approximately equal to 2.7. Qualitative results showed expected behavior regarding formation of shear-layer flow, rise of oscillations, and growth in instabilities such as K-H and R-T. To characterize quantitatively, estimations of spray angle, droplet diameter and ligament length were also made. Moreover, the constructed atomizer proved to be a suitable method for the analysis proposed for this study.

5. ACKNOWLEDGEMENTS

The authors are grateful for the financial support of PETROBRAS for this research project, through the cooperation agreement number 5850.0107354.18.9. This study was financed in part by the Coordenação de Aperfeiçoamento de Pessoal de Nível Superior – Brasil (CAPES) – Finance Code 001. A special thanks to Dayvid Anderson Setter, whose contribution was key to complete this work, and many other people who helped directly and indirectly.

6. REFERENCES

- Cui, J., Lai, H., Li, J. and Ma, Y., 2017. “Visualization of internal flow and the effect of orifice geometry on the characteristics of spray and flow field in pressure-swirl atomizers”. *Applied Thermal Engineering*, Vol. 127, p. 812-822. 30 Jul 2020 < <http://dx.doi.org/10.1016/j.applthermaleng.2017.08.103>>.
- Davanlou, A., Lee, J. D., Basu, s. and Kumar, R., 2015. “Effect of viscosity and surface tension on breakup and coalescence of bicomponent sprays”. *Chemical Engineering Science*, Vol 131, p. 243-255. 28 Jul 2020 <<http://dx.doi.org/10.1016/j.ces.2015.03.057>>.
- Ghasemi, A., Li, X., Hong, Z. and Yun, S., 2020. “Breakup mechanisms in air-assisted atomization of highly viscous pyrolysis oils”. *Energy Conversion And Management*, Vol 220, p. 113-122. 27 Jul 2020 <<http://dx.doi.org/10.1016/j.enconman.2020.113122>>.
- Hopfinger, E. J., 1998. “Liquid jet instability and atomization in a coaxial gas stream”. *Fluid Mechanics and its applications: Advances in Turbulence VII*, Vol 46, p. 69-78, 09 Sep 2020 < https://doi.org/10.1007/978-94-011-5118-4_17>.

- Kundu, P. K., Cohen, I. M. and Dowling, D. R., 2012. *Fluid Mechanics*. Academic Press, Waltham, 5th edition.
- Lasheras, J. C. and Hopfinger, E. J., 2000. "Liquid jet instability and atomization in a coaxial gas stream". *Annual Review Of Fluid Mechanics*, Vol 32, p. 275-308, 09 Sep 2020 < <https://doi.org/10.1146/annurev.fluid.32.1.275>>.
- Lefebvre, A. H. and McDonnell, V. G., 2017. *Atomization and Sprays*. CRC Press, Boca Raton, 2nd edition.
- Murugan, R., Kolhe, P. S., Sahu, K. C., 2020. "A combined experimental and computational study of flow-blurring atomization in a twin-fluid atomizer". *European Journal Of Mechanics – B/Fluids*, 30 Jul 2020 < <http://dx.doi.org/10.1016/j.euromechflu.2020.07.008>>.
- Sadeghbeigi, R., 2012. *Fluid Catalytic Cracking Handbook: An Expert Guide to the Practical Operation, Design, and Optimization of FCC Units*. Elsevier, Waltham, 3rd edition.
- Saha, A., Lee, J. D., Basu, s. and Kumar, R., 2012. "Breakup and coalescence characteristics of a hollow cone swirling spray". *Physics Of Fluids*, Vol. 24, p. 124103. 25 Jul 2020 <<http://dx.doi.org/10.1063/1.4773065>>.
- Sens, M., Maass, J., Wirths, S. and Marohn, R., 2012. "Effects of highly-heated fuel and/or high injection pressures on the spray formation of gasoline direct injection injectors". *Fuel Systems for IC Engines*, p. 215-238. 31 Jul 2020 < <http://dx.doi.org/10.1533/9780857096043.6.215>>.
- Sharp, D.H., 1984. "An overview of Rayleigh-Taylor instability". *Physica D: Nonlinear Phenomena*, Vol. 12. 30 Jul 2020 <[http://dx.doi.org/10.1016/0167-2789\(84\)90510-4](http://dx.doi.org/10.1016/0167-2789(84)90510-4)>.

7. RESPONSIBILITY NOTICE

The authors are the only responsible for the printed material included in this paper.